RSC Advances

PAPER

View Article Online
View Journal | View Issue

Cite this: *RSC Adv.*, 2024, **14**, 24055

Fabrication of a novel nanofiltration membrane using an Mg–Fe layered double hydroxide for dye/salt separation†

Xiuzhen Wei, *[a] Zelong Chen,[a] Mengjia He,[a] Liangliang Xu,[a] Yue Li,[b] Jia Yang,[c] Xuekang Zhang,[a] Xianghao Zhang,[a] Ze Wang,[a] Shiyu Cao,[a] Qinghua Zhou*[a] and Bingjun Pan *[a]

Mg–Fe layered hydroxide (LDH) was synthesized by the double titration method and added to trimesoyl chloride (TMC) to prepare an Mg–Fe LDH-modified polyamide nanofiltration (NF) membrane by interfacial polymerization (IP). Compared to the pure polyamide NF membrane, the Mg–Fe LDH-modified membrane presented a wrinkled structure and a comparatively smooth surface. Additionally, the permeation flux and rejection rate of the modified NF membrane for 1000 mg L^{-1} Na_2SO_4 solution were 61.7 L m^{-2} h^{-1} and 95.9%, respectively. When the Mg–Fe LDH modified NF membrane was used to separate dye/NaCl mixed solutions, the rejection of NaCl was less than 17% and the rejection rate of Coomassie Brilliant Blue (CBB) molecules was close to 100%. At the same time, the concentration of CBB increased from 500 mg L^{-1} to 1151 mg L^{-1} which means that the LDH modified NF membrane could separate CBB/NaCl effectively and could concentrate CBB at the same time.

Received 7th May 2024
Accepted 21st July 2024

DOI: 10.1039/d4ra03366c

rsc.li/rsc-advances

1 Introduction

For decades, industrial wastewater treatment has been a very important and widely studied issue. The more complex the composition of wastewater, the more stable the pollutants are, and the more difficult it is to treat, such as the textile industry's wastewater. Approximately 70% of the wastewater in the entire textile industry comes from printing and dyeing wastewater.[1] Some of these dye molecules will migrate into the environment through various dye production processes and use channels. Due to their stable chemical properties and low level of degradability, dyeing wastewater causes severe pollution to the ecological environment, potentially harming animals, plants, and even humans. Normally, dyeing wastewater contains high concentrations of inorganic salts such as NaCl,[2] which are used to improve the absorption of dyes by fabrics,[3] thus making the biodegradation of dyeing wastewater more difficult and the treatment process more complex. If NaCl and dye molecules in dye wastewater can be separated and recycled, not only will the amount of wastewater be significantly reduced, but the wastewater will also be more easily biodegraded, which will achieve greater economic benefits.

Membrane separation technology has shown great advantages in molecular separation and wastewater treatment due to its high efficiency, energy savings, and environmental protection characteristics.[4] Among them, nanofiltration (NF) membranes can retain organic compounds with 200–1000 Da molecular weights through Donnan repulsion and pore-size exclusion, exhibiting enormous potential in the separation of dyes and salts for wastewater treatment.[5] Jabbarvand Behrouz's study showed that TFC-NF membranes have good desalination performance at low pressure.[6] LNMs membranes prepared using polysulfone (PSF) membranes functionalized with L-histidine amino acids showed good dye separation performance.[7] Simultaneously, the rejection rate of cationic dyes by PEI-NF membranes in the treatment of dyeing wastewater is more than 95%.[7] The relative results indicated that NF membranes could effectively remove relatively large dyeing molecules from dyeing wastewater. However, Chen's studies indicated that[8] some dyeing molecules and inorganic salt molecules were rejected at the same time and that dyeing molecules could not be completely separated from NaCl molecules. The effective separation of dyeing molecules and NaCl molecules faces huge challenges.

Traditional NF membranes generally have low permeation flux, poor antifouling properties, short service life, and poor

[a]College of Environment, Zhejiang University of Technology, Hangzhou, 310014, China. E-mail: qhzhou@zjut.edu.cn; bjpan@zjut.edu.cn; xzwei@zjut.edu.cn
[b]Abbey College Cambridge, Cambridge, Cambridgeshire, UK
[c]Ninghai Society of Environmental Science and Technology, Ningbo, Zhejiang, 315600, China

† Electronic supplementary information (ESI) available: The element mapping images and FTIR spectra of Mg–Fe LDH; the wide-scan XPS analysis spectra of different NF membranes; the influence of membrane preparation conditions, including the concentration of PIP, TMC, Mg–Fe LDH, heat treatment time, and heat treatment temperature, were optimized based on the permeation flux and rejection rate for 1000 mg L^{-1} Na_2SO_4 solution. See DOI: https://doi.org/10.1039/d4ra03366c

NaCl and dye separation performance, which also limit the development and application of NF membranes in dyeing wastewater treatment.[9] Thus, nanoparticles, such as ZnO/*y*-FeOOH NP_S,[10] GO,[11] sulfonated GO/ZnO nanocomposites,[12] and multiwall carbon nanotube (MWCNT),[13] were utilized to enhance the flux and antifouling properties of NF membranes. Nanoparticle modified NF membranes improved their rejection behavior for small organic molecules such as sulfamethoxazole, and some modified NF membranes exhibited photocatalytic properties in some degree. However, the modification still did not realize the effective separation of dye and NaCl molecules. Layered double hydroxide (LDH)[14,15] has received increasing attention in recent years due to its distinctive properties, such as large specific surface area, nontoxicity, easy preparation, and good stability.

LDH is an ionic compound with a layered structure. It is a compound made up of interlayer anions and positively charged layers that assemble in an ordered manner.[14] The chemical formula can be written as $[M_{1-x}^{2+}M_x^{3+}(OH)_2]^{x+}(A^{n-})_{x/n}\cdot mH_2O$, and M^{2+} M^{3+}, and A^{n-} are the divalent cation, trivalent metal cation, and exchangeable intercalation anion, respectively.[16] By changing the types and proportions of metal ions and the types of anions, the physical and chemical properties of LDH are changed, which could lead to the change of NF membranes properties. The antifouling ability and chlorine resistance of NF membrane were significantly enhanced by blending MgAl–CO_3 LDH nanomaterials.[17] NiCo-LDH/PVDF ultrafiltration composite membranes with novel high-performance and grass-like structures were prepared which could efficiently separate various oil-water emulsions.[18] The antifouling and photocatalytic properties of NF membranes were improved by doping Zn/Al LDH into the polyamide layer during the IP process.[19] The permeation flux and rejection behavior of PA NF membranes were improved by adding Cu/Al LDH.[20] To date, most studies on LDH have focused on aluminum-containing or cobalt-containing (Co) LDH, such as magnesium–aluminum,[21] copper–aluminum, cobalt–nickel,[18] and cobalt–aluminum.[15,22] However, Al^{3+} in LDH may enter the water body through isomorphous replacement, which may cause potential harm to humans. Although Co is considered as the most effective transition metal for pollutant degradation, it precipitates readily from water bodies and is highly toxic and harmful to ecosystems. Most importantly, magnesium and iron are essential elements for human life activities, and Fe is environmentally friendly, nontoxic and efficient. The use of Mg and Fe to prepare double hydroxides has good ecological compatibility and is more suitable for green development. In addition, Mg–Fe layered hydroxide (Mg–Fe LDH) has many positive charges and abundant surface hydroxyl groups and interlayer hydroxyl groups, which can interact with polymer molecules to form an LDH-modified composite NF membrane with good hydrophilicity and antifouling properties. Thus, NF membranes modified by Mg–Fe LDH may reject organic compounds with 200–1000 Da molecular weights such as dyes molecules effectively through Donnan repulsion and pore-size exclusion and can let NaCl molecules permeate through NF membrane realizing the effectively separation of dyes and NaCl for wastewater treatment. What's more, no Mg–Fe LDH-modified NF membranes have been reported to date.

Mg–Fe LDH was synthesized and its morphology and structure were characterized by scanning electron microscopy (SEM), X-ray diffraction (XRD), Fourier transform infrared spectroscopy (FTIR), and X-ray photoelectron spectroscopy (XPS). Mg–Fe LDH was added into trimesoyl chloride (TMC) to prepare Mg–Fe LDH-modified polyamide NF membranes by IP. NF membrane preparation conditions were optimized, and the surface morphology of the prepared NF membranes was characterized by SEM and atomic force microscopy (AFM). The surface chemical structure and composition of the NF membranes were analyzed by EDX, XPS and FTIR. Additionally, the hydrophilicity and separation performance of NF membranes were also studied.

2 Experimental

2.1 Material

Trimesoyl chloride (TMC) and Piperazine (PIP) were obtained from Aladdin Reagent Co; *N*-hexane, absolute ethanol, and sodium hydroxide (NaOH) were purchased from Chinese Medicine Group Chemical Reagent Co., Ltd. (Beijing, China); Polyethylene glycol (PEG, C.P. grade) were purchased from Shanghai Qiangshun Chemical Reagent Co., Ltd.; ferric chloride hexahydrate ($FeCl_3\cdot 6H_2O$), magnesium sulfate ($MgSO_4$), sodium sulfate (Na_2SO_4,), magnesium chloride hexahydrate ($MgCl_2\cdot 6H_2O$), sodium chloride (NaCl) and sodium carbonate (Na_2CO_3) were obtained from Chengdu Kelong chemical reagent Factory; Coomassie Brilliant Blue ($C_{47}H_{48}N_3NaO_7S_2$, CBB) has a relative molecular mass of 854.02 g mol^{-1} and a maximum absorption wavelength is 584 nm. The water used in the research is laboratory-made ultrapure water. Polysulfone (PSF) ultrafiltration (UF) membrane (MWCO, 50 000) was supplied by RisingSun Membrane Technology (Beijing) Co., Ltd. Unless otherwise noted, all compounds were analytical grade and used without any further purification.

2.2 Preparation and characterization of Mg–Fe LDH

Mg–Fe LDH was prepared by the double titration method. 0.1 mol L^{-1} $MgCl_2\cdot 6H_2O$ and 0.1 mol L^{-1} $FeCl_3\cdot 6H_2O$ at a volume ratio of 3 : 1 was mixed to make salt solution A. 0.4 mol L^{-1} NaOH and 0.2 mol L^{-1} Na_2CO_3 were mixed to make alkali solution B. Then, alkali solution B was slowly added to vigorously stirred solution A at 80 °C, and the final pH was controlled to be 11–12. After the titration was completed, the mixture was stirred vigorously for 30 min, allowed to stand for 4 hours and then centrifuged. The precipitate was washed repeatedly with pure water and absolute ethanol. The precipitate was dried in an oven at 105 °C for 12 hours to obtain Mg–Fe LDH. The sample was kept in a desiccator for further use.

2.3 Preparation and characterization of Mg–Fe LDH composite NF membranes

A PSF flat UF membrane was employed as a substrate to fabricate Mg–Fe LDH-modified composite NF membrane. A 0.3 wt%

PIP aqueous solution (7 : 3, pure water to absolute ethanol) was poured onto PSF UF surface and kept for approximately 10 minutes. The excess solution was then drained, and pure nitrogen gas was used to dry the UF membrane. Next, some Mg–Fe LDH dispersed into a 0.15 wt% TMC/*n*-hexane solution, and the mixture was contacted with the UF membrane surface for 50 s to obtain the LDH-modified composite NF membrane. The new NF membranes were then dried and kept in deionized (DI) water for further use. The optimization of NF membrane preparation conditions is described in the Online Resource (Table S1†). The effect of PIP concentration, TMC concentration, Mg–Fe LDH concentration and heat treatment conditions on NF membrane properties were shown in ESI.†

SEM (SIRION-100, Holland FEI) was applied to analyze the morphology of the composite NF membrane. All samples were coated with a thin layer of gold under vacuum before observation. ATR-FTIR (Nicolet6700, American Thermo Fisher) was used to analyze the chemical structure of the NF membranes. All spectra were acquired from 450 to 4000 cm^{-1} with 32 scans at a resolution of 2.0 cm^{-1}. Using an Al X-ray source, XPS (Thermo Fisher, USA) was used to examine the chemical composition of the membrane. The water contact angle of different membranes was measured with 1 μL of water at 25 °C using a contact angle goniometer (CA, OCA20, Dataphysiscs, Germany), and the measurements were repeated at least five times to assess the membrane's hydrophilicity. The surface roughness was evaluated using atomic force microscopy (AFM, SP13800N, American Veeco Precision Instrument Co., Ltd.). The scanning area was 4 μm × 4 μm.

2.4 Separation performance characterization of the NF membrane

2.4.1 NF membrane permeation performance. Cross-flow filtration equipment was used to test NF membrane separation properties and the effective membrane area was 24 cm^2. NF membranes were stabilized using DI water for 0.5 hours at 0.4 MPa before testing. A feed of DI water or solutions containing different solutes, such as $MgSO_4$, Na_2SO_4, NaCl, $MgCl_2$, and PEG, were used to test the performance of the NF membrane. The concentrations of the different solutions were all 1000 mg L^{-1}. The permeation and rejection solutions were recycled back into the feed solution to keep the concentration constant. The temperature was kept constant at 25.0 °C and 0.4 MPa for the entirety of NF separation performance. The results of parallel experiments were repeated at least three times to verify reproducibility.

According to eqn (1), the permeation flux of the NF membrane was calculated.

$$F = V/(A \times t) \quad (1)$$

where F is the permeate flux, L m^{-2} h^{-1}, t is the operation time (h), A is the effective permeation area (m^2), and V is the volume of permeate (L).

Eqn (2) was used to determine the rejection rate.

$$R = (1 - C_p/C_f) \times 100\% \quad (2)$$

where C_P and C_f (mg L^{-1}) represent the feed and permeate solution concentrations, respectively.

A total organic carbon analyzer was used to measure the PEG solution concentrations (TOC-V CPN, Shimadzu, Japan). The salt concentration is obtained by measuring the conductivity, which can be acquired by the conductivity meter DDSJ-308A (Shanghai Precision Scientific Instruments Co., Ltd., China).

2.4.2 Dye/salt separation properties of NF membrane. A dye/salt mixed solution was used as simulated dyeing wastewater to examine the separation performance of the NF membrane for various dyeing wastewater. The NF membrane was operated for 30 min with pure water at 0.4 MPa until the membrane reached a stable state. The pH of the mixture was approximately 7, and all NF separation performance was performed at 0.4 MPa.

The mixture solutions of dye (Coomassie Brilliant Blue (CBB)) and salt (NaCl) were 500 and 10 000 mg L^{-1}, respectively. The feed solution was divided into a permeate solution and a concentrated solution by NF separation equipment. The process lasted for approximately 4.5 h, and the permeate volume, conductivity, and absorbance of the permeate solution and the feed solution were tracked and measured every 30 minutes. A TU-1810 ultraviolet-visible spectrophotometer was used to characterize the concentration of CBB.

2.4.3 Molecular weight cutoff (MWCO) and pore size distribution. PEG with a known molecular weight was used to characterize the membrane's molecular weight cutoff. The PEG used in this study had molecular weights of 200, 400, 600, 800, and 1000 Da, and its concentration was 1000 mg L^{-1}. A total organic carbon (TOC) analyzer was used to determine the amount of PEG in the feed and permeate solution. The following density function (eqn (3)) can be used to express the pore size distribution of the NF membrane.[23]

$$dR(d_p)/d(d_p) = 1/d_p \ln \sigma_p\sqrt{2\pi}\cdot\exp\left[\left(\ln d_p - \ln \mu_p\right)^2/2\left(\ln \sigma_p\right)^2\right] \quad (3)$$

where d_p represents the diameter of the membrane pore, nm; μ_p represents the solute radius when the rejection rate was 50%, nm; σ_p represents the ratio of the solute radius when the rejection rate was 83.14% to the solute radius when the rejection rate was 50%.

The rejection rate and the solute radius have the following relationship (eqn (4)).

$$F(R_T) = A + B \ln r_s \quad (4)$$

where R_T represents the solute rejection rate, %; r_s represents the radius of the solute, nm.

According to the above logarithmic curve, the values of σ_p and μ_p can be calculated. Moreover, according to the research results of Meireles *et al.*,[24] eqn (5) provides the relationship between the molecular weight of PEG and its molecular radius and the molecular radius of different PEG are shown in Table S2.†

$$r_s = 16.73 \times 10^{-12} \times M_w^{0.557} \quad (5)$$

M_w represents the relative molecular mass of PEG, g mol^{-1}.

3 Results and discussion

3.1 Characterization of Mg–Fe LDH and Mg–Fe LDHm

The morphological structure of the Mg–Fe LDH and Mg–Fe LDH membrane (LDHm) were well characterized by scanning electron microscopy (SEM). The surface morphology of Mg–Fe LDH nanoparticles is shown in Fig. 1a and b. As it can be seen, Mg–Fe LDH nanoparticles present a relative perfect sheet-like structure with uniform crystal grain size and clearly boundaries. The elemental composition of Mg–Fe LDH was analyzed by EDS, and the results showed that Mg, Fe, O and C were uniformly distributed in the nanoparticles (Fig. S1†). The results indicated that Mg–Fe LDH nanoparticles were synthesized successfully and that Mg/Fe was uniformly distributed in the synthesized nanomaterials.

Meanwhile, the surface and cross section morphologies of different membranes were characterized and the results were shown in Fig. 1c–f. PA-0 surface showed a granular modular structure (Fig. 1c), which was the typical morphology of NF membranes prepared by PIP and TMC.[25,26] Noticeably, the PA-2 surface presented a wrinkled structure (Fig. 1d). Compared with PA-0, a more complicated fold structure appears on the PA-2 surface, and the surface becomes relatively smoother. The thickness of the selective layer of PA-2 was thinner than that of PA-0, which was consistent with the change in membrane surface structure (Fig. 1e and f). This phenomenon may be attributed to the hydrophilicity of LDH. Due to the hydration effect, LDH will swell in certain extent in water.[27–29] When the organic phase containing LDH and TMC contacts the water phase containing PIP molecules, the hydration of LDH leads some water molecules to penetrate into *n*-hexane, which increases the diffusion coefficient of PIP molecules.[30] Additionally, the diffusion of PIP monomers can be sped up by the release of hydration heat.[31] Therefore, the presence of LDH in the organic phase during interfacial polymerization led to an increase in the reaction area and endowed the membranes with a leaf-like morphology. Additionally, Mg–Fe LDH interferes with IP procedure and reduces the thickness of the functional layer. The PA-2 membrane surface was analyzed by SEM-EDX to investigate the distribution of Mg–Fe LDH nanoparticles in the NF membrane selective layer and the results are shown in Fig. 1g. Carbon (C), oxygen (O), nitrogen (N), magnesium (Mg), and iron (Fe) are distributed uniformly on the PA-2 NF membrane surface, which also proves that Mg–Fe LDH distributed uniformly in the selective layer of NF membrane.

The crystal structure and phase composition of the prepared Mg–Fe LDH were analyzed by X-ray diffraction (XRD), and the symmetric and sharp diffraction peaks of the material can be seen in Fig. 2a, which indicated that the synthesized Mg–Fe LDH had high crystallinity. The degrees of the diffraction peaks are 11.5°, 23.7°, 34.3°, 39.2°, 46.3°, 59.6°, and 61.5° correspond to the (0 0 3), (0 0 6), (0 1 2), (0 1 5), (0 1 8), (1 1 0), and (1 1 3) crystal planes, which are in agreement with the standard peaks of the characteristic features of Mg–Fe LDH materials (JCPDS no. 33-0869).[14,25,32,33] The XRD characterization of Mg–Fe LDHm presented the same signal peaks on the membrane surface,

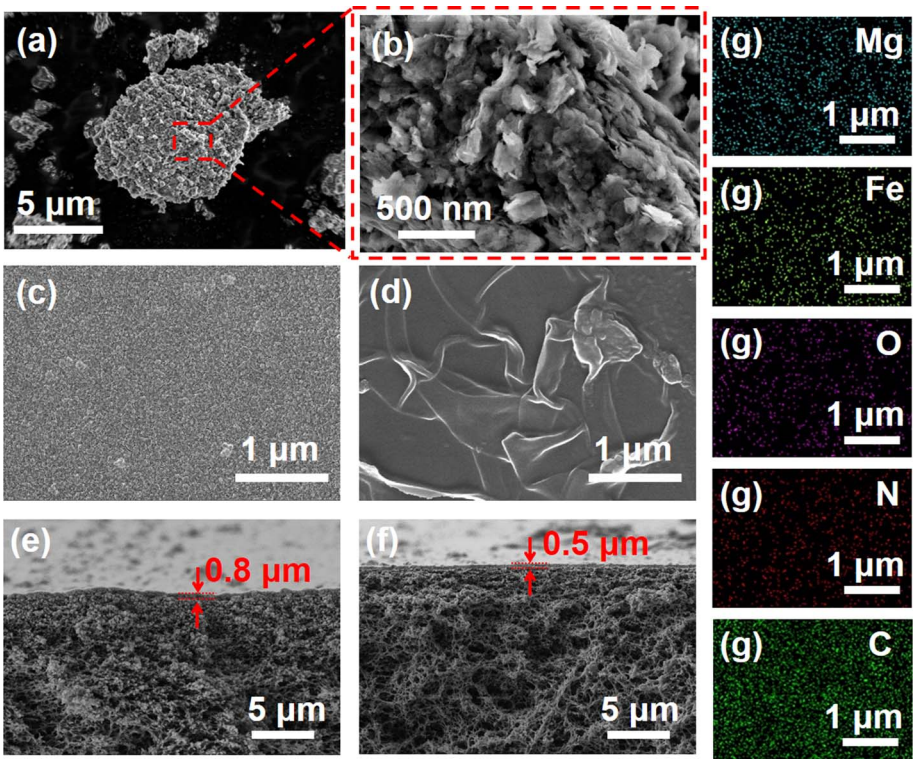

Fig. 1 (a and b) SEM image of Mg–Fe LDH; surface SEM images of (c) PA-0 and (d) PA-2; cross-section image of (e) PA-0 and (f) PA-2; (g) EDS mapping of PA-2 membrane with respect to Mg, Fe, O, N, and C.

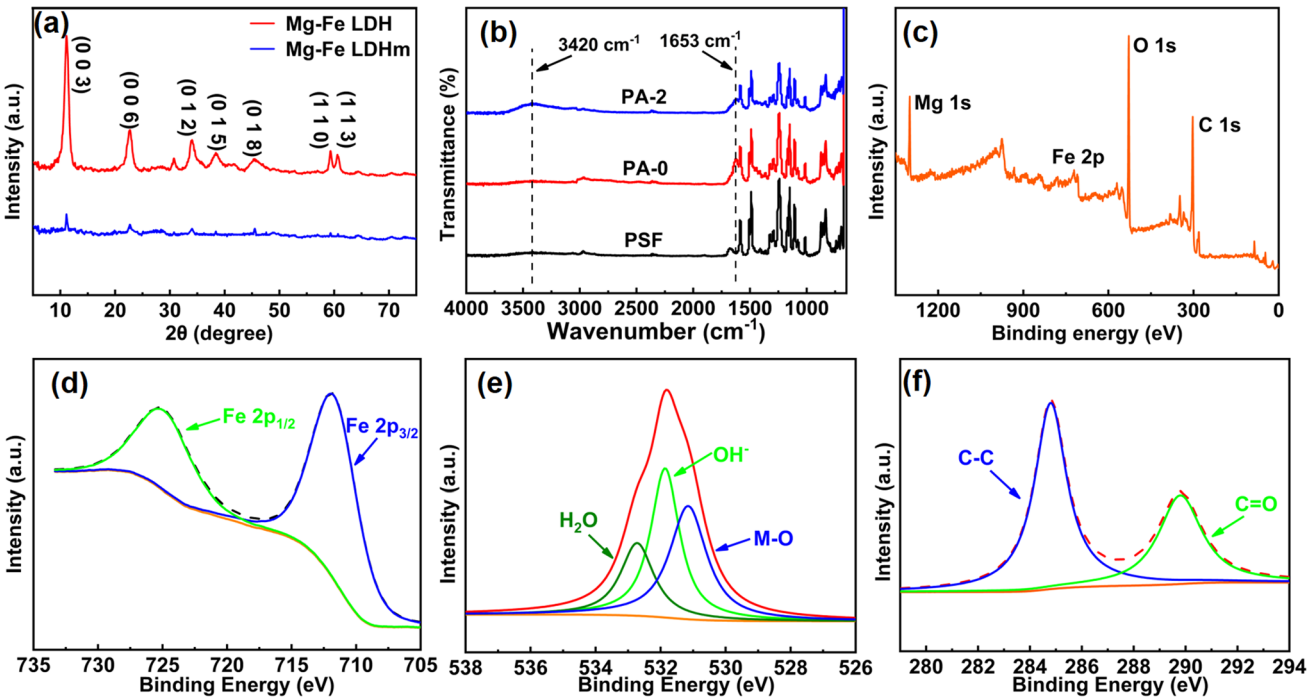

Fig. 2 (a) XRD pattern of Mg–Fe LDH and Mg–Fe LDHm; (b) FTIR spectroscopy of PSF UF substrate and NF membranes, PA-0, PA-2; XPS spectra of Mg–Fe LDH: (c) wide spectra; (d) Fe 2p; (e) O 1s; (f) C 1s.

which indicated that Mg–Fe LDH was successfully composited onto PSF-UF membrane surface by interfacial polymerization.

As seen in Fig. 2b, new characteristic peaks at 1653 cm^{-1} and 3420 cm^{-1} emerged in comparison to the PSF support membrane. The peak at 1653 cm^{-1} was the stretching vibration peak of the –CONH– group produced by the IP reaction, and the broad absorption peak at 3420 cm^{-1} was due to the presence of the –OH group.[34] These results indicate that a new PA layer was formed on PSF membrane surface. Mg–Fe LDH contains a large number of hydrophilic –OH groups, which makes PA-2 present a relative stronger absorption peak at 3420 cm^{-1}, which favors the hydrophilicity of the NF membrane. However, there are no absorption peaks of Mg and Fe for PA-2. This may be due to Mg and Fe are inorganic elements, and their absorption is not obvious. On the other hand, the concentration of Mg–Fe LDH in NF membranes is relatively low. The prepared Mg–Fe LDH was also analyzed by FTIR spectroscopy (Fig. S2†) and the telescopic vibrational peak observed at 3435 cm^{-1} can be attributed to the hydroxyl groups (–OH) on the Mg–Fe LDH flakes.[14,35] In addition, the bending vibrational peak observed at 1640 cm^{-1} belongs to the –OH group in the crystal water, since water molecules are adsorbed on the surface and between the layers of Mg–Fe LDH.[36] Another strong absorption band at 1000–500 cm^{-1} corresponds to the stretching vibration of the interlayer carbonate anion in the LDH support. The low-frequency absorption band is attributed to the metal–oxygen group. An Mg–O bond absorption peak was formed at 1487 cm^{-1} and a Fe–O bond absorption peak was showed at 580 cm^{-1}.[37,38]

X-ray photoelectron spectroscopy (XPS) was used to characterize the chemical composition and valence state of different elements in Mg–Fe LDH and the results are shown in Fig. 2c. The photoelectron peaks of Mg 1s, Fe 2p, O 1s, and C 1s were found in the survey spectrum. The split peak results of Fe 2p are shown in Fig. 2d and two peaks appeared at 711.7 eV and 724.9 eV, which corresponded to the $2p_{3/2}$ and $2p_{1/2}$ states of metallic Fe, respectively. The binding energy difference of 13.2 eV indicates that Fe in Mg–Fe LDH presented in the form of +3 valence.[39–41] As shown in Fig. 3e, the O 1s spectrum was divided into three peaks at 530.9 eV, 531.8 eV, and 532.8 eV, which represented O in the oxide (replaced by MO). The –OH group on the surface is the physical or chemical structure of the water in the sample.[42] As shown in Fig. 3f, the C 1s high-resolution spectrum show electron peaks at the binding energies of 284.6 eV and 289.8 eV, representing the contaminated carbon and the C=O in the sample, respectively. Meanwhile, the chemical compositions of the different membranes were characterized by XPS. It can be seen from Fig. S3† that the PA-2 and PA-4 membranes had obvious characteristic peaks of Mg 1s compared to PA-0, while the characteristic peaks of Fe 2p are not obvious due to the lower concentration of Mg–Fe LDH. The results showed in Fig. S3 and Table S3† indicated that Mg and Fe are present on the surface of the NF membranes with a Mg : Fe content ratio of about 3 : 1, suggesting that the Mg–Fe LDH was successfully entrapped into the selective layer of the NF membranes.

Three-dimensional morphology and surface roughness of different membranes were investigated using atomic force microscopy (AFM). The scanning area was 4 μm × 4 μm, and Fig. 3 displayed 2D and 3D surface images of three NF membranes. All NF membranes have the typical "peaks and

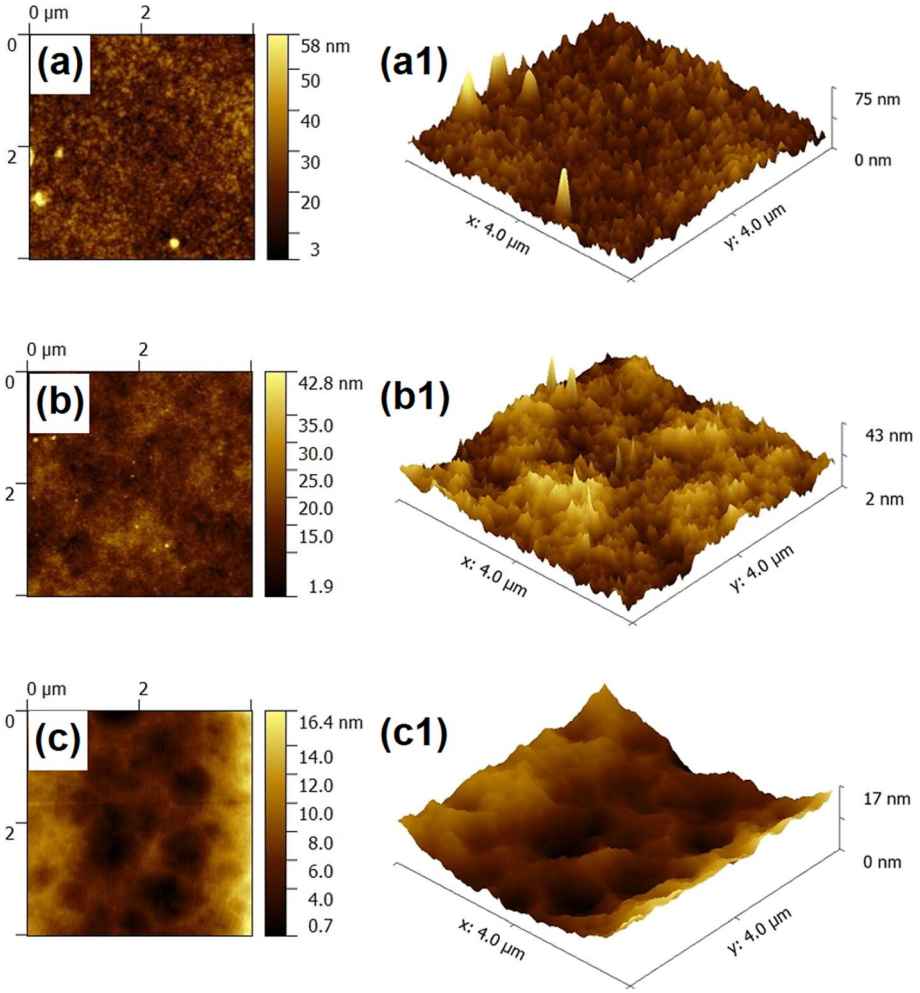

Fig. 3 2D (a–c) and 3D (a1–c1) AFM surface images of the PA-0, PA-2 and PA-4.

valleys" characteristic structure of polyamide NF membranes. Average roughness (Ra) and root mean square roughness are two metrics used to describe the surface roughness of the NF membrane (RMS). Table S4† shown that the surface roughness of the NF membrane gradually decreases as the Mg–Fe LDH concentration increases. The Ra value decreased from 4.99 nm to 2.43 nm, and the RMS value decreased from 6.58 nm to 2.98 nm. Compared to PA-0, the valleys likewise rose while the hills were flattened for PA-2 and PA-4. The decreased surface roughness may be the result of hydrogen bonding between the polyamide layer and the functional groups of the Mg–Fe LDH composite. A smoother surface might also result from adding Mg–Fe LDH to the surface's troughs or deeper areas.[43,44] Additionally, the single ridge presented in PA-2 has a larger planer area that corresponds to the leaf-like surfaces of the modified membranes. This phenomenon was consistent with the results of SEM characterization for different NF membrane surfaces. A relatively smooth surface can reduce the adhesion and deposition of pollutants during wastewater treatment, which endows the NF membrane with relatively stronger antifouling performance.

3.2 Apparent properties of Mg–Fe LDHm

The hydrophilicity of the different membranes was evaluated by water contact angle measurements. As shown in Fig. 4a, the water contact angle decreased from 35.5° to 10.7° with the increase of Mg–Fe LDH concentration, which indicated that the introducing of Mg–Fe LDH nanoparticles enhanced the hydrophilicity of NF membrane. Hydrophilic NF membranes can attract water molecules close to their surfaces and promote the permeation of water molecules through the membranes. Moreover, a hydration layer would be formed on the hydrophilic membrane surface to resist the adhesion and deposition of pollutants. This endows the modified NF membrane with relatively better permeability and antifouling properties. The pure water flux of different NF membranes is shown in Fig. 4b. As the concentration of Mg–Fe LDH increased from 0 to 0.20 wt%, the pure water flux of the NF membrane increased from 30.1 L m^{-2} h^{-1} to 80.8 L m^{-2} h^{-1}, and the pure water flux of PA-4 is approximately 2.7 times that of PA-0. The increase in flux is mainly due to the following three reasons. (1) The addition of Mg–Fe LDH enhances the hydrophilicity of the NF membrane, which lead the NF membrane surface can absorb more water

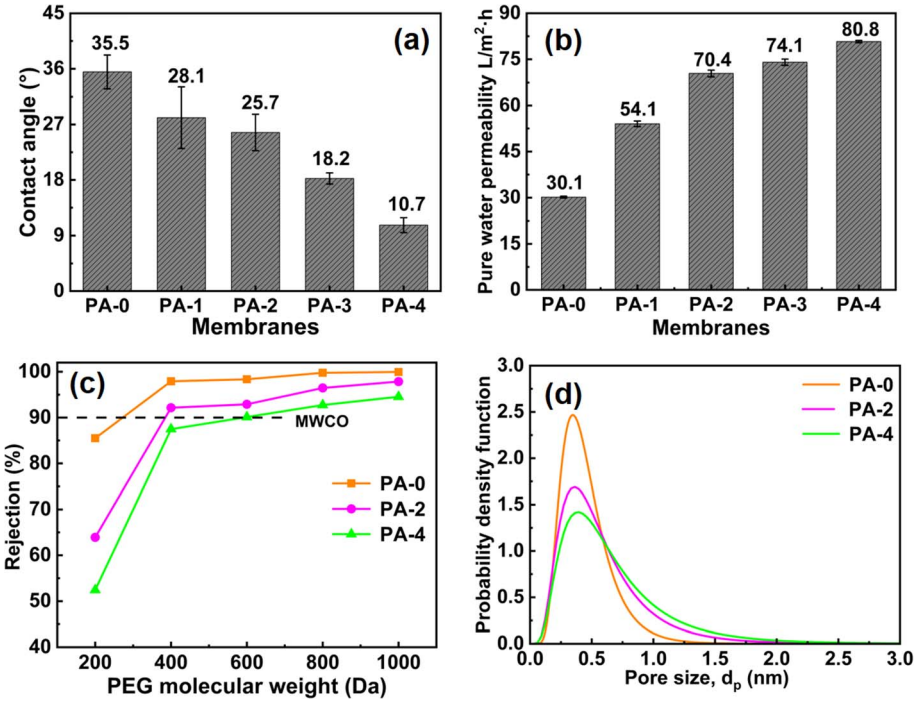

Fig. 4 (a) Surface water contact angle of different NF membranes; (b) pure water flux of different NF membranes; (c) rejection rates of the prepared PA-0, PA-2 and PA-4 membranes to PEG with different molecular weights; (d) probability density function curve for the bore diameter of PA-0, PA-2 and PA-4 membranes.

molecules resulting in easier penetration of water molecules; (2) the unique layered structure of Mg–Fe LDH provided abundant interlayer channels, which endows additional water molecule transmission channels;[45] (3) the fold structure shown on the modified NF membrane surface enhances the filtration area where water molecules can effectively contact the NF membrane.

The molecular weight cut-off values of NF membranes were obtained by measuring the rejection rates of different NF membranes for different molecular weight PEGs. As shown in Fig. 4c and Table S5,† the molecular weight cutoffs of PA-0, PA-2, and PA-4 were 281, 385, and 597 Da, respectively. The average effective pore size and pore size distribution were calculated using the solute migration model, and the results showed that the average effective pore size of the NF membranes increased slightly with the increase of Mg–Fe LDH concentration (Fig. 4d and Table S5†). This phenomenon was attributed to the fact that embedding Mg–Fe LDH into the PA matrix interfered with the reaction between the amine group and the acyl chloride group, which decreased the cross-linking degree of the selective layer. In addition, due to the incompatibility between Mg–Fe LDH and polymers, some defects may be formed on the selective layer during the IP reaction. These results are consistent with the XPS results.

3.3 Separation properties of Me–Fe LDHm

3.3.1 Separation performance of the NF membrane for inorganic salts. Penetration flux and inorganic rejection rate were used to evaluate the separation performance of different NF membrane. As shown in Fig. 5a, the permeation flux rose constantly when the LDH concentration increased from 0 to 0.2 wt%. The rejection rate order of all NF membranes to four inorganic salts is as follows: Na_2SO_4 > $MgSO_4$ > $MgCl_2$ > NaCl (Fig. 5b). This rejection pattern suggested that the modified NF membrane showed a negative charge.[46] Compared with PA-0, the rejection rate of the NF membrane modified by LDH decreased slightly, and the decline degree also increased with LDH concentration increasing. When the LDH concentration was 0.2 wt% (PA-4), the rejection rates for Na_2SO_4 > $MgSO_4$ > $MgCl_2$ > NaCl were 93.7%, 87.6%, 22.1%, and 19.1%, respectively, which are close to that of PA-0. The introduction of LDH increased the average pore size of the NF membranes, which led to an increase in the permeation flux and a decrease in the rejection rate. Moreover, some defects in the selective layer of the NF membrane may be formed during the IP reaction process due to the existence of LDH. Furthermore, LDH nanoparticles embedded in the selective layer may be exposed on the NF membrane surface and come into contact with the electrolyte solution, leading to more positive charges on the membrane surface.[41] Therefore, the quantity of negative charges on the modified membrane surface under neutral conditions is reduced, which reduces the Donnan repulsion effect to a certain extent.[46] For PA-2, the permeation flux and rejection rate of Na_2SO_4 was 60.6 L m^{-2} h^{-1} and 96.4%, respectively. Compared with PA-0, the rejection rate for Na_2SO_4 did not change obviously, and the flux significantly increased by approximately 255%.

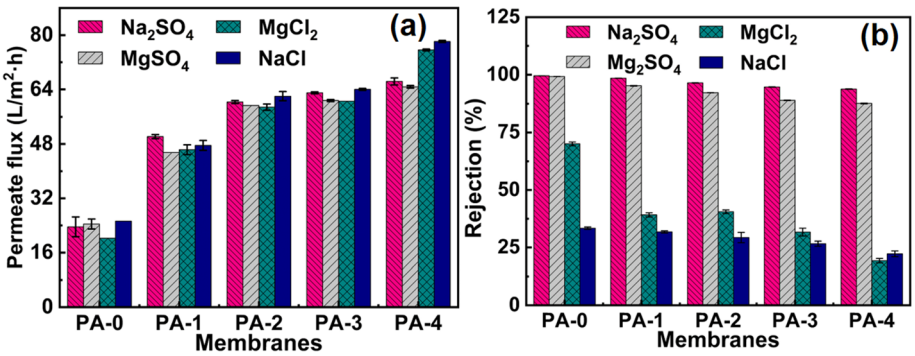

Fig. 5 Permeate flux (a) and rejection rates (b) of different NF membranes for inorganic salts.

3.3.2 Operation stability of Mg–Fe LDH-modified NF membrane. The stability of the NF membrane separation performance determines whether it can be used in practical applications. In Fig. 6a, the separation performance of the PA-0 and PA-2 membranes was tested for 60 h continuously to characterize the separation performance stability. The permeation flux of PA-2 is 60 L m^{-2} h^{-1}, and the rejection rate is 95%. The permeation flux of PA-0 is 25 L m^{-2} h^{-1}, and the rejection rate is 99%. The PA-2 membrane has a similar rejection rate to PA-0, but the permeation flux of PA-2 is 2.4 times that of PA-0. Both membranes showed a very stable permeation flux and rejection rate in the continuous 60 h operation, indicating that the polyamide structure of the NF membrane was very stable and the Mg–Fe LDH-modified NF membrane could be used in practical applications.

The permeation flux and rejection rate of different membranes to Na_2SO_4 are compared (Fig. 6b and Table S6†), and the results showed that the Mg–Fe LDH-modified NF membranes prepared in this study present apparent advantages in permeability and rejection performance. The NF membrane modified by adding Mg–Fe LDH to the organic phase *n*-hexane presents higher rejection rate while maintaining better permeation flux due to the special layered structure and the abundant hydrophilic groups of Mg–Fe LDH. The modified NF membrane fabricated in this study exhibits obvious advantages in permeation flux and salt rejection compared to the modified NF membrane described in the literature, indicating that the modified NF membrane has good application potential in water treatment. Moreover, the permeation flux of NF270 (a commercial NF membrane) under the same test conditions is only 30.9 L m^{-2} h^{-1}, and the rejection rate was 93.6%.[47]

3.3.3 Separation of dye/salt by NF membrane. Mg–Fe LDH modified NF membrane shows a higher permeation flux and a lower rejection rate for NaCl, which can be used to separate dye/NaCl mixed solutions. PA-2 and PA-0 are used to treat CBB/NaCl mixed solution, and the results are shown in Fig. 7. As shown in Fig. 7a, the concentration of CBB in the feed solution rose from 500 mg L^{-1} to 1151 mg L^{-1}, and its concentration increased by 2.3 times after the mixed solution was treated for 4.5 hours using PA-2. Additionally, the concentration of NaCl in the feed solution rose from 10 000 mg L^{-1} to 11 720 mg L^{-1}. Even after 4.5 h of continuous concentration, the permeation flux of the PA-2 membrane remained at approximately 55.0 L m^{-2} h^{-1}, the removal rate of CBB remained above 99.2%, and the removal rate of NaCl remained below 17% (Fig. 7b). The results showed that PA-2 can reject most CBB molecules and let most NaCl molecules permeate through the NF membrane, which means PA-2 can effectively separate the CBB/NaCl mixed solution, and the separation performance can remain stable. However, after the mixed solution was treated with the PA-0 membrane for 4.5 hours (Fig. 7c and d), the concentration of CBB increased from 500 mg L^{-1} to 758 mg L^{-1}, suggesting that the concentration effect of CBB by PA-0 was not very obvious. Moreover, during the whole operation process, the permeation flux for PA-0 was only approximately 25 L m^{-2} h^{-1}. The permeation flux of PA-2 membrane was 2.2 times that of the

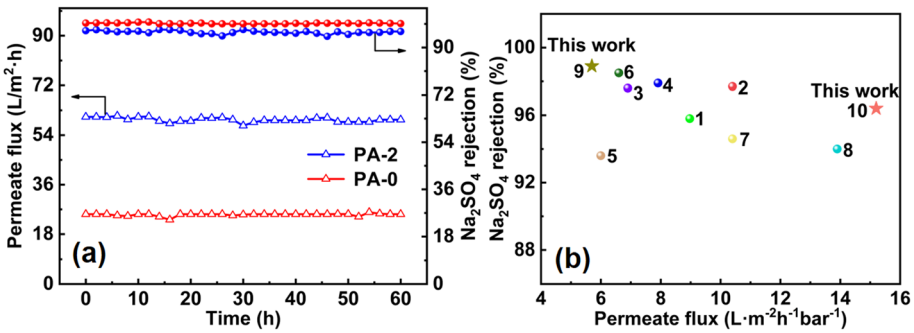

Fig. 6 (a) Separation performance stability of different NF membranes; (b) Na_2SO_4 rejection rate comparison of different NF membranes.

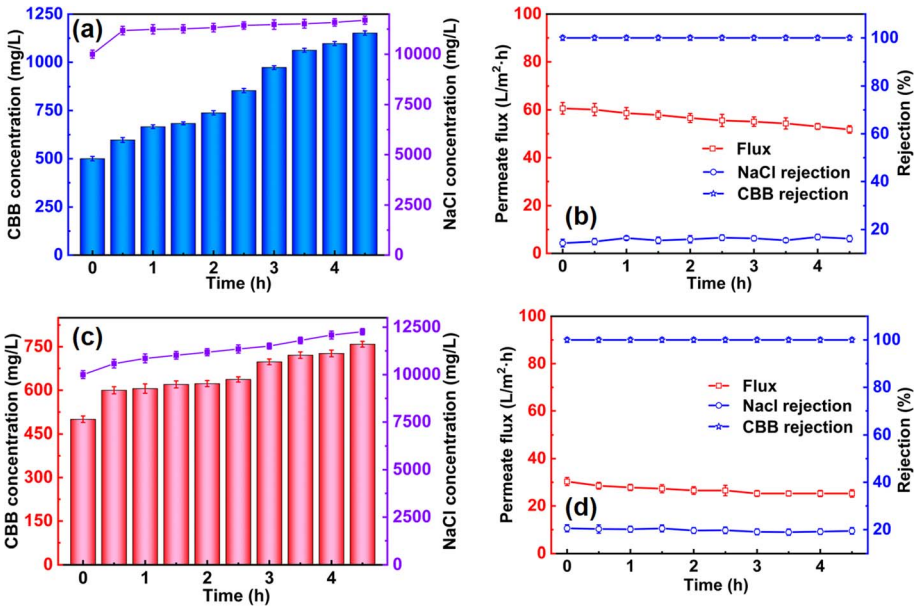

Fig. 7 Concentration change of feed solution and NF separation performance of different membranes during concentration process (4 bar, 25 °C, 500 mg L^{-1} CBB and 10 000 mg L^{-1} NaCl): (a) and (b) for PA-2; (c) and (d) for PA-0.

PA-0 membrane while showing a similar rejection rate with that of the PA-0 membrane. PA-2 can effectively reject most CBB molecules and let most NaCl molecules permeate through the NF membrane and the separation performance can remain stable. This indicated that the modified NF membrane has a suitable pore size and pore size distribution, which guarantees that when water and NaCl molecules penetrate through the NF membrane, CBB molecules are effectively rejected. The results show that the NF membrane modified by Mg–Fe LDH is more suitable for separating dye/NaCl mixed solutions.

4. Conclusion

Mg–Fe LDH with a layered structure and many –OH groups was synthesized by the double precipitation method, and Mg–Fe-LDH was added to *n*-hexane to prepare a polyamide NF membrane by the IP reaction process. When the concentration of Mg–Fe LDH is 0.1 wt% (PA-2), the prepared NF membrane shows the best separation performance. The rejection rate of PA-2 to 1000 mg L^{-1} Na_2SO_4 solution was 95.9%, and the permeation flux was 60.7 L m^{-2} h^{-1}. The modified NF membrane shows good operation stability, and after 60 hours of continuous operation, the permeability and rejection performance of the NF membrane remain unchanged. The Mg–Fe LDH modified NF membrane has excellent NaCl/dye separation performance. The rejection rate of the modified NF membrane for 500 mg L^{-1} CBB is close to 100%, and the rejection rate for 10 000 mg L^{-1} NaCl is less than 17%. NF membranes' apparent rejection rate difference for dye and NaCl molecules makes the modified NF membrane suitable for separating NaCl and dye mixed solutions. This means that the Mg–Fe LDH-modified polyamide NF membrane has good application prospects in separating and reusing high-concentration NaCl/dye wastewater.

Ethical statement

No humans or animals were involved in this study.

Data availability

The data supporting this article have been included within the manuscript and its ESI.†

Author contributions

Xiuzhen Wei: supervision, writing – review & editing. Zelong Chen and Ze Wang: formal analysis, writing – original draft, conceptualization. Mengjia He and Shiyu Cao: validation. Liangliang Xu: data curation. Yue Li: validation. Jia Yang and Xuekang Zhang: formal analysis. Xianghao Zhang: resources. Qinghua Zhou: project administration. Bingjun Pan: project administration. All authors have read and agreed to the published version of the manuscript.

Conflicts of interest

The authors declare that there is no conflict of interest and competing interest.

Acknowledgements

This work was supported by the Natural Science Foundation of Zhejiang Province (Grant No. LY20B070009) and the National Natural Science Foundation of China (No. 42277275).

References

1 Y. Tu, G. Shao, W. Zhang, J. Chen, Y. Qu, F. Zhang, S. Tian, Z. Zhou and Z. Ren, The degradation of printing and dyeing wastewater by manganese-based catalysts, *Sci. Total Environ.*, 2022, **828**, 154390.

2 L. X. Liu, L. Yu, B. Borjigin, Q. Y. Liu, C. W. Zhao and D. Y. Hou, Fabrication of thin-film composite nanofiltration membranes with improved performance using beta-cyclodextrin as monomer for efficient separation of dye/salt mixtures, *Appl. Surf. Sci.*, 2021, **539**, 148284.

3 J. Lin, W. Ye, H. Zeng, H. Yang, J. Shen, S. Darvishmanesh, P. Luis, A. Sotto and B. Van der Bruggen, Fractionation of direct dyes and salts in aqueous solution using loose nanofiltration membranes, *J. Membr. Sci.*, 2015, **477**, 183–193.

4 M. A. Abdel-Fatah, Nanofiltration systems and applications in wastewater treatment: review article, *Ain Shams Eng. J.*, 2018, **9**(4), 3077–3092.

5 J. Y. Lin, Q. Chen, X. Huang, Z. S. Yan, X. C. Lin, W. Y. Ye, S. Arcadio, P. Luis, J. H. Bi, B. van der Bruggen and S. F. Zhao, Integrated loose nanofiltration-electrodialysis process for sustainable resource extraction from high-salinity textile wastewater, *J. Hazard. Mater.*, 2021, **419**, 126505.

6 S. Jabbarvand Behrouz, A. Khataee, M. Safarpour, S. Arefi-Oskoui and S. Woo Joo, Carboxymethyl cellulose/polyethersulfone thin-film composite membranes for low-pressure desalination, *Sep. Purif. Technol.*, 2021, **269**, 118720.

7 S. Jabbarvand Behrouz, A. Khataee, V. Vatanpour and Y. Orooji, Surface Bioengineering of Mo_2Ga_2C MAX Phase to Develop Blended Loose Nanofiltration Membranes for Textile Wastewater Treatment, *ACS Appl. Mater. Interfaces*, 2024, **16**(8), 10508–10521.

8 P. Chen, X. Ma, Z. Zhong, F. Zhang, W. Xing and Y. Fan, Performance of ceramic nanofiltration membrane for desalination of dye solutions containing NaCl and Na_2SO_4, *Desalination*, 2017, **404**, 102–111.

9 D. Yadav, S. Karki and P. G. Ingole, Current advances and opportunities in the development of nanofiltration (NF) membranes in the area of wastewater treatment, water desalination, biotechnological and pharmaceutical applications, *J. Environ. Chem. Eng.*, 2022, **10**(4), 108109.

10 G. Moradi, M. Rahimi, S. Zinadini and S. Hadidi, Fabrication of the polyethersulfone/functionalized mesoporous carbon nanocomposite nanofiltration membranes for dyes and heavy metal ions removal: experimental and quantum mechanical simulation method, *Polym. Adv. Technol.*, 2023, **34**(1), 89–109.

11 L. Yang, F. C. Jia, Z. G. Juan, D. H. Yu, L. Y. Sun, Y. Song, Y. X. Wang, L. J. Huang and J. G. Tang, High-permeable graphene oxide/graphitic carbon nitride composite nanofiltration membrane for selective separation of dye and desalination, *J. Environ. Chem. Eng.*, 2023, **11**(2), 109306.

12 G. Boopathy, A. Gangasalam and A. Mahalingam, Photocatalytic removal of organic pollutants and self-cleaning performance of PES membrane incorporated sulfonated graphene oxide/ZnO nanocomposite, *J. Chem. Technol. Biotechnol.*, 2020, **95**(11), 3012–3023.

13 X. Z. Wei, S. Y. Cao, J. Y. Hu, Y. Chen, R. Y. Yang, J. H. Huang, Z. Wang, Q. H. Zhou and J. Y. Chen, Graphene oxide/multi-walled carbon nanotubes nanocomposite polyamide nanofiltration membrane for dyeing-printing wastewater treatment, *Polym. Adv. Technol.*, 2021, **32**(2), 690–702.

14 A. E. A. Aboubakr, W. M. A. El Rouby, M. D. Khan, A. A. Farghali and N. Revaprasadu, ZnCr-CO_3 LDH/ruptured tubular g-C_3N_4 composite with increased specific surface area for enhanced photoelectrochemical water splitting, *Appl. Surf. Sci.*, 2020, **508**, 145100.

15 R. Guo, Y. Zhu, X. Cheng, J. Li and J. C. Crittenden, Efficient degradation of lomefloxacin by Co-Cu-LDH activating peroxymonosulfate process: optimization, dynamics, degradation pathway and mechanism, *J. Hazard. Mater.*, 2020, **399**, 122966–122976.

16 L. Peng, N. Yang, Y. Yang, Q. Wang, X. Xie, D. Sun-Waterhouse, L. Shang, T. Zhang and G. I. N. Waterhouse, Atomic cation-vacancy engineering of NiFe-Layered double hydroxides for improved activity and stability towards the oxygen evolution reaction, *Angew. Chem., Int. Ed.*, 2021, **60**(46), 24612–24619.

17 P. Lu, W. Li, S. Yang, Y. Liu, Q. Wang and Y. Li, Layered double hydroxide-modified thin–film composite membranes with remarkably enhanced chlorine resistance and anti-fouling capacity, *Sep. Purif. Technol.*, 2019, **220**, 231–237.

18 J. Cui, Z. Zhou, A. Xie, Q. Wang, S. Liu, J. Lang, C. Li, Y. Yan and J. Dai, Facile preparation of grass-like structured NiCo-LDH/PVDF composite membrane for efficient oil–water emulsion separation, *J. Membr. Sci.*, 2019, **573**, 226–233.

19 Y. Mutharasi, N. J. Kaleekkal, T. Arumugham, F. Banat and M. S. R. S. Kapavarapu, Antifouling and photocatalytic properties of 2-D Zn/Al layered double hydroxide tailored low-pressure membranes, *Chem. Eng. Process.: Process Intensif.*, 2020, **158**, 108191–108203.

20 F. Zhong, P. Q. Wang, Y. He, C. L. Chen, H. J. Li, H. Yu and J. Y. Chen, Preparation of stable and superior flux GO/LDH/PDA-based nanofiltration membranes through electrostatic self-assembly for dye purification, *Polym. Adv. Technol.*, 2019, **30**(7), 1644–1655.

21 E. Abdollahi, A. Heidari, T. Mohammadi, A. A. Asadi and M. A. Tofighy, Application of Mg-Al LDH nanoparticles to enhance flux, hydrophilicity and antifouling properties of PVDF ultrafiltration membrane: experimental and modeling studies, *Sep. Purif. Technol.*, 2021, **257**, 117931–117943.

22 R. Guo, Y. Li, Y. Chen, Y. Liu, B. Niu, J. Gou and X. Cheng, Efficient degradation of sulfamethoxazole by CoCu LDH composite membrane activating peroxymonosulfate with decreased metal ion leaching, *Chem. Eng. J.*, 2021, **417**, 127887–127900.

23 C.-E. Lin, J. Wang, M.-Y. Zhou, B.-K. Zhu, L.-P. Zhu and C.-J. Gao, Poly(m-phenylene isophthalamide) (PMIA): a potential polymer for breaking through the selectivity-

permeability trade-off for ultrafiltration membranes, *J. Membr. Sci.*, 2016, **518**, 72–78.

24 M. Meireles, A. Bessieres, I. Rogissart, P. Aimar and V. Sanchez, An appropriate molecular size parameter for porous membranes calibration, *J. Membr. Sci.*, 1995, **103**(1–2), 105–115.

25 X. Liu, G. Liu, W. Y. Li, Q. Y. Wang and B. L. Deng, Effects of the substrate on interfacial polymerization: tuning the hydrophobicity via polyelectrolyte deposition, *Membranes*, 2020, **10**(10), 259–278.

26 J. Zhu, S. Yuan, A. Uliana, J. Hou, J. Li, X. Li, M. Tian, Y. Chen, A. Volodin and B. V. der Bruggen, High-flux thin film composite membranes for nanofiltration mediated by a rapid co-deposition of polydopamine/piperazine, *J. Membr. Sci.*, 2018, **554**, 97–108.

27 N. Iyi, K. Fujii, K. Okamoto and T. Sasaki, Factors influencing the hydration of layered double hydroxides (LDHs) and the appearance of an intermediate second staging phase, *Appl. Clay Sci.*, 2007, **35**(3–4), 218–227.

28 X. Li, Z. Yu, L. Shao, H. Zeng, Y. Liu and X. Feng, A novel strategy to construct a visible-light-driven Z-scheme (ZnAl-LDH with active phase/g-C_3N_4) heterojunction catalyst via polydopamine bridge (a similar "bridge" structure), *J. Hazard. Mater.*, 2020, **386**, 121650–121665.

29 Y. Cao, D. Zheng, F. Zhang, J. Pan and C. Lin, Layered double hydroxide (LDH) for multi-functionalized corrosion protection of metals: a review, *J. Mater. Sci. Technol.*, 2022, **102**, 232–263.

30 Y. Zhao, N. Li and S. Xia, Polyamide nanofiltration membranes modified with Zn–Al layered double hydroxides for natural organic matter removal, *Compos. Sci. Technol.*, 2016, **132**, 84–92.

31 H. Dong, L. Wu, L. Zhang, H. Chen and C. Gao, Clay nanosheets as charged filler materials for high-performance and fouling-resistant thin film nanocomposite membranes, *J. Membr. Sci.*, 2015, **494**, 92–103.

32 P. Koilraj and S. Kannan, Aqueous fluoride removal using ZnCr layered double hydroxides and their polymeric composites: batch and column studies, *Chem. Eng. J.*, 2013, **234**, 406–415.

33 R. Guo, Y. Zhu and X. Cheng, Efficient degradation of lomefloxacin by Co-Cu-LDH activating peroxymonosulfate process: optimization, dynamics, degradation pathway and mechanism, *J. Hazard. Mater.*, 2020, **399**, 122966.

34 X. Tian, J. Wang, H. Zhang, Z. Cao, M. Zhao, Y. Guan and Y. Zhang, Establishment of transport channels with carriers for water in reverse osmosis membrane by incorporating hydrotalcite into the polyamide layer, *RSC Adv.*, 2018, **8**(22), 12439–12448.

35 L. H. Zhang, F. Li, D. G. Evans and X. Duan, Structure and surface characteristics of Cu-based composite metal oxides derived from layered double hydroxides, *Mater. Chem. Phys.*, 2004, **87**(2–3), 402–410.

36 X. M. Peng, M. Wang, F. P. Hu, F. X. Qiu, T. Zhang, H. L. Dai and Z. Cao, Multipath fabrication of hierarchical CuAl layered double hydroxide/carbon fiber composites for the degradation of ammonia nitrogen, *J. Environ. Manage.*, 2018, **220**, 173–182.

37 Z. Gao, R. F. Xie, G. L. Fan, L. Yang and F. Li, Highly efficient and etable bimetallic AuPd over La-doped Ca-Mg-Al layered double hydroxide for base-free aerobic oxidation of 5-hydroxymethylfurfural in water, *ACS Sustainable Chem. Eng.*, 2017, **5**(7), 5852–5861.

38 Y. D. Guo, Z. H. Gong, C. X. Li, B. Gao, P. Li, X. G. Wang, B. C. Zhang and X. M. Li, Efficient removal of uranium (VI) by 3D hierarchical Mg/Fe-LDH supported nanoscale hydroxyapatite: a synthetic experimental and mechanism studies, *Chem. Eng. J.*, 2020, **392**, 123682–123695.

39 B. Ou, J. X. Wang, Y. Wu, S. Zhao and Z. Wang, Efficient removal of Cr (VI) by magnetic and recyclable calcined CoFe-LDH/g-C_3N_4 via the synergy of adsorption and photocatalysis under visible light, *Chem. Eng. J.*, 2020, **380**, 122600–122611.

40 A. Kumar, A. Rana, G. Sharma, M. Naushad, A. H. Al-Muhtaseb, C. S. Guo, A. Iglesias-Juez and F. J. Stadler, High-performance photocatalytic hydrogen production and degradation of levofloxacin by Wwide spectrum-responsive Ag/Fe_3O_4 bridged $SrTiO_3$/g-C_3N_4 plasmonic nanojunctions: joint effect of Ag and Fe_3O_4, *ACS Appl. Mater. Interfaces*, 2018, **10**(47), 40474–40490.

41 L. F. Cui, D. Zhao, Y. Yang, Y. X. Wang and X. D. Zhang, Synthesis of highly efficient alpha-Fe_2O_3 catalysts for CO oxidation derived from MIL-100(Fe), *J. Solid State Chem.*, 2017, **247**, 168–172.

42 J. Zhu, Y. Zhu and W. Zhou, Cu-doped Ni-LDH with abundant oxygen vacancies for enhanced methyl 4-hydroxybenzoate degradation via peroxymonosulfate activation: key role of superoxide radicals, *J. Colloid Interface Sci.*, 2022, **610**, 504–517.

43 M. Safarpour, V. Vatanpour, A. Khataee and M. Esmaeili, Development of a novel high flux and fouling-resistant thin film composite nanofiltration membrane by embedding reduced graphene oxide/TiO_2, *Sep. Purif. Technol.*, 2015, **154**, 96–107.

44 Y. Zhao, N. Li, F. Yuan, H. Zhang and S. Xia, Preparation and characterization of hydrophilic and antifouling poly(ether sulfone) ultrafiltration membranes modified with Zn-Al layered double hydroxides, *J. Appl. Polym. Sci.*, 2016, **133**(39), 43988–43997.

45 R. Hu, Y. He, C. Zhang, R. Zhang, J. Li and H. Zhu, Graphene oxide-embedded polyamide nanofiltration membranes for selective ion separation, *J. Mater. Chem. A*, 2017, **5**(48), 25632–25640.

46 G. Ribera, L. Llenas, M. Rovira, J. de Pablo and X. Martinez-Llado, Pilot plant comparison study of two commercial nanofiltration membranes in a drinking water treatment plant, *Desalin. Water Treat.*, 2012, **51**(1–3), 448–457.

47 Y. Wang, Z. X. Yang, L. Liu and Y. B. Chen, Construction of high performance thin-film nanocomposite nanofiltration membrane by incorporation of hydrophobic MOF-derived nanocages, *Appl. Surf. Sci.*, 2021, **570**, 151093–151102.